

# Conditional modulation of spike–timing–dependent plasticity for olfactory learning

Stijn Cassenaer<sup>1,2</sup> & Gilles Laurent<sup>1,3</sup>

**Mushroom bodies are a well-known site for associative learning in insects. Yet the precise mechanisms that underlie plasticity there and ensure their specificity remain elusive. In locusts, the synapses between the intrinsic mushroom body neurons and their postsynaptic targets obey a Hebbian spike–timing–dependent plasticity (STDP) rule. Although this property homeostatically regulates the timing of mushroom body output, its potential role in associative learning is unknown. Here we show *in vivo* that pre–post pairing causing STDP can, when followed by the local delivery of a reinforcement–mediating neuromodulator, specify the synapses that will undergo an associative change. At these synapses, and there only, the change is a transformation of the STDP rule itself. These results illustrate the multiple actions of STDP, including a role in associative learning, despite potential temporal dissociation between the pairings that specify synaptic modification and the delivery of reinforcement–mediating neuromodulator signals.**

Behavioural and genetic experiments in *Drosophila* and honeybees have revealed that the mushroom body, a brain area containing up to hundreds of thousands of neurons called Kenyon cells, is critical for associative learning of odours<sup>1–11</sup> but not for the expression of innate odour-driven behaviours<sup>5</sup> (Fig. 1a). Recent electrophysiological experiments in locusts and other insects show that the responses of Kenyon cells to odours are highly selective and, thus, rare<sup>12–14</sup>. By contrast, antennal lobe neurons, the source of the olfactory input to Kenyon cells, are few and promiscuous<sup>12</sup>. Odour codes are thus ‘compact’ in the antennal lobe—that is, the representation of each odour engages many neurons in a small population—but ‘sparse’ in the mushroom bodies (Fig. 1a). Although sparse codes require larger neuron populations, they are beneficial for memory because they can reduce interference between memory traces<sup>12,15,16</sup>. Kenyon cells project to two regions, called  $\alpha$ - and  $\beta$ -lobes, where they synapse onto small populations of ‘extrinsic’ neurons. In locusts, the synapses between Kenyon cells and  $\beta$ -lobe neurons (bLNs) are modifiable by a Hebbian STDP rule<sup>17–19</sup> (Fig. 1a), but nothing so far implicates STDP in associative learning there; rather, STDP causes the homeostatic regulation of bLN spike timing<sup>17</sup>. Recent experimental results in moths<sup>14</sup> show that Kenyon cell responses to odours recorded during behavioural learning generally occur and end well before reward delivery, indicating that STDP alone cannot support associative conditioning<sup>20,21</sup>. Neuromodulation has been proposed recently as a potential solution<sup>22,23</sup>. We address this issue with *in vivo* electrophysiology in locusts and discover a complex interplay between STDP, reinforcer signals and odour codes in mushroom bodies.

## Dense odour representations in $\beta$ -lobes

We first examine odour representations in the  $\beta$ -lobes. Using intradendritic recordings, we sampled the responses of 55 bLNs to up to 16 odours (Methods and Fig. 1b). Each bLN responded to nearly every odour, with responses that differed in intensity, patterning, delay and duration across neuron–odour pairs. The probability that a given bLN responded to an odour was 0.97. On average, a bLN fired action potentials in approximately half of the local field potential (LFP) oscillation cycles during the odour presentation ( $0.502 \pm 0.219$ ,  $n = 126$

neuron–odour pairs, 25 LFP cycles per response): on average, half of the population was active in any given cycle. Hence, these representations resemble those in the antennal lobes<sup>12</sup> (and exceed them in promiscuity) rather than the sparse representations by Kenyon cells, to which bLNs are directly connected.

We tested whether the broad tuning of bLNs might be explained by known features of mushroom body circuits. We implemented a simple model (Methods and ref. 17) constrained by Kenyon cell response statistics and timing<sup>12</sup>, by the properties of STDP at Kenyon cell synapses<sup>17</sup> and by Kenyon cell/bLN (KC–bLN) connectivity ratios estimated from experiments<sup>17</sup>. With such a model, we could reproduce the bLN firing phase observed experimentally<sup>17</sup> (Fig. 2a, left) but not the odour-response intensity or probability (Fig. 2a, right, and Supplementary Fig. 1.1a). Rather, activity across the model bLN (mbLN) population saturated rapidly when STDP was turned on. This behaviour is a known property of rate-based Hebbian learning in model networks and can be counteracted by imposing synaptic weight bounds or renormalization rules<sup>24</sup>.

## Inhibition limits STDP and saturation

In examining our experimental data on bLN responses to odours, we observed that the periodic excitatory input originating from Kenyon cells was often curtailed by phasic inhibitory postsynaptic potentials (Fig. 2b, arrowheads), with onsets at the typical phase of bLN action potentials. We hypothesized that these inhibitory postsynaptic potentials originate from lateral inhibition among bLNs (as put forward in a theoretical exploration<sup>25</sup>). This was supported by extracellular stimulation of Kenyon cells (Supplementary Fig. 2) and confirmed in paired bLN recordings. Beta-lobe neurons inhibit each other (Fig. 2c) with an estimated connection probability of 28% ( $n = 32$  connections, 2 reciprocally connected pairs). Although unknown so far, other interneuron populations may also contribute to bLN inhibition.

In each oscillation cycle, lateral inhibition reduces the likelihood of late bLN spikes; thus, it should limit the ability of STDP to potentiate KC–bLN synapses. This in turn should curb bLN population activity (see also ref. 26). As predicted, implementing lateral inhibition

<sup>1</sup>Division of Biology, California Institute of Technology, Pasadena, California 91125, USA. <sup>2</sup>Broad Fellows Program in Brain Circuitry, California Institute of Technology, Pasadena, California 91125, USA. <sup>3</sup>Max Planck Institute for Brain Research, 60528 Frankfurt am Main, Germany.

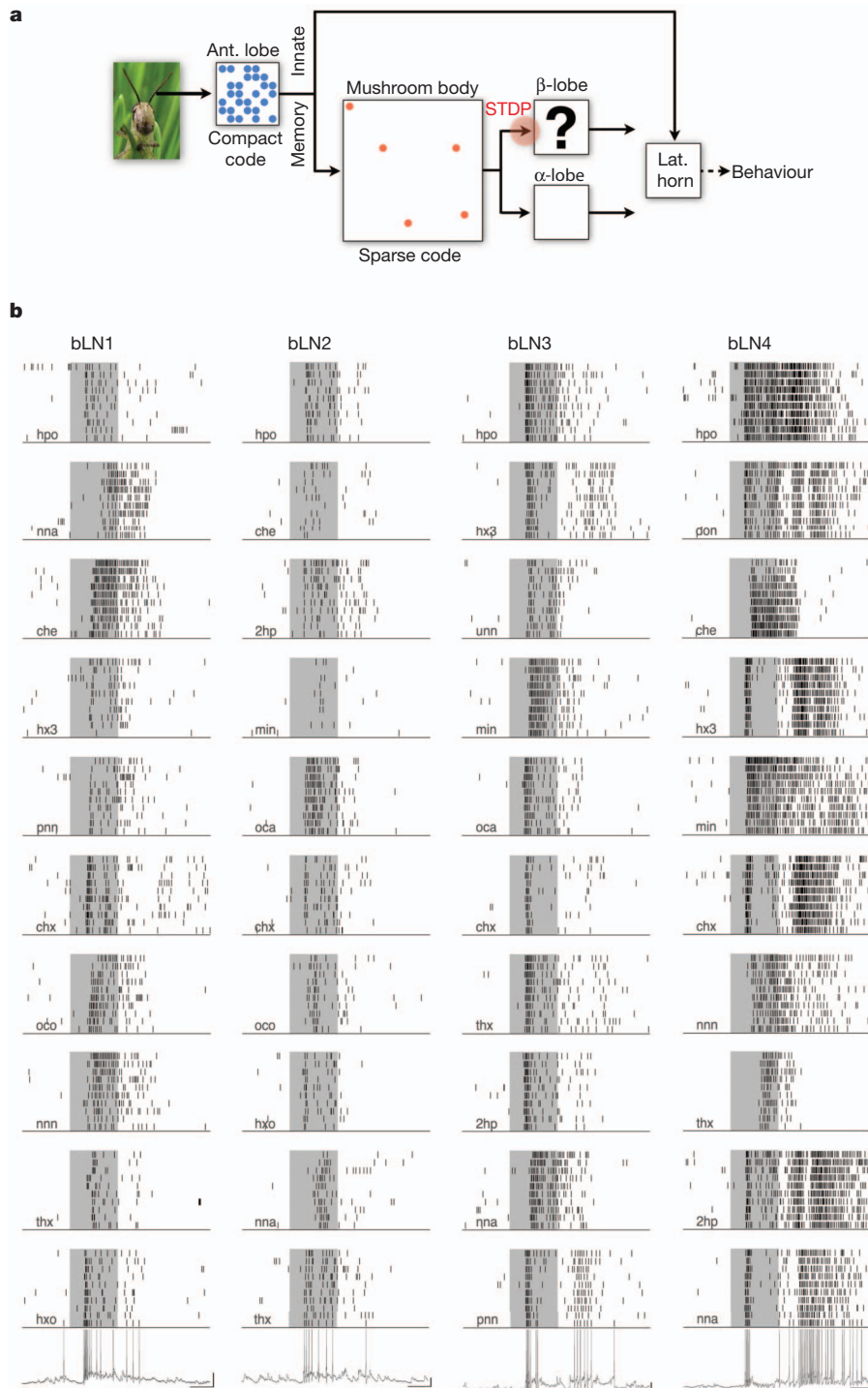


**Figure 1 | Beta-lobe neurons are promiscuous.** **a**, Olfactory circuit in which bLNs are embedded. Ant., antenna; lat., lateral. **b**, Rasters constructed from *in vivo* intracellular dendritic recordings, illustrating responses of four bLNs (different animals) to ten odours. Shaded region represents odour delivery (1 s). For each bLN, intracellular traces at bottom correspond to the tenth trial with the last odour.

Horizontal scale bars, 500 ms; vertical scale bars, 10 mV; spikes are clipped. Odours: 2-heptanone (2hp), cherry (che), *cis*-3-hexen-1-ol (chx), 3,7-dimethyl-2,6-octadiene-nitrile (don), 1-heptanol (hpo), 1-hexen-3-ol (hx3), 1-hexanol (hxo), mint (min), nonanal (nna), 5-nonanone (nnn), octanal (oca), 1-octanol (oco), 3-pentanone (pnn), *trans*-2-hexen-1-ol (thx), 6-undecanone (unn).

between mbLNs (based on the experimental connectivity estimate and amplitude distribution) reduced population activity to  $\sim 50\%$  ( $p_{\text{response}} = 0.51 \pm 0.14$  (response probability),  $n = 30$  mbLNs; compare with  $p_{\text{response}} = 0.49 \pm 0.18$ ,  $n = 30$  bLNs from experiment; Fig. 2d–f). The mbLN spike phase remained centred on  $\pi$  (LFP trough). In addition, the response profiles of those mbLNs were very similar to those recorded experimentally (compare distributions in Fig. 2e, f and moments in Fig. 2g; see also Supplementary Figs 3–5).

We conclude that bLN activity, although very different from the sparse output of Kenyon cells, can be explained by the combined effects of Hebbian STDP at KC–bLN synapses and lateral inhibition between bLNs. The useful consequences are that bLN spikes are tightly phase-locked to the LFP<sup>17</sup> and that instantaneous bLN population activity lies around the midpoint of its dynamic range. This increases the coding capacity of this small population of output neurons and is relevant for plasticity, as explored below.

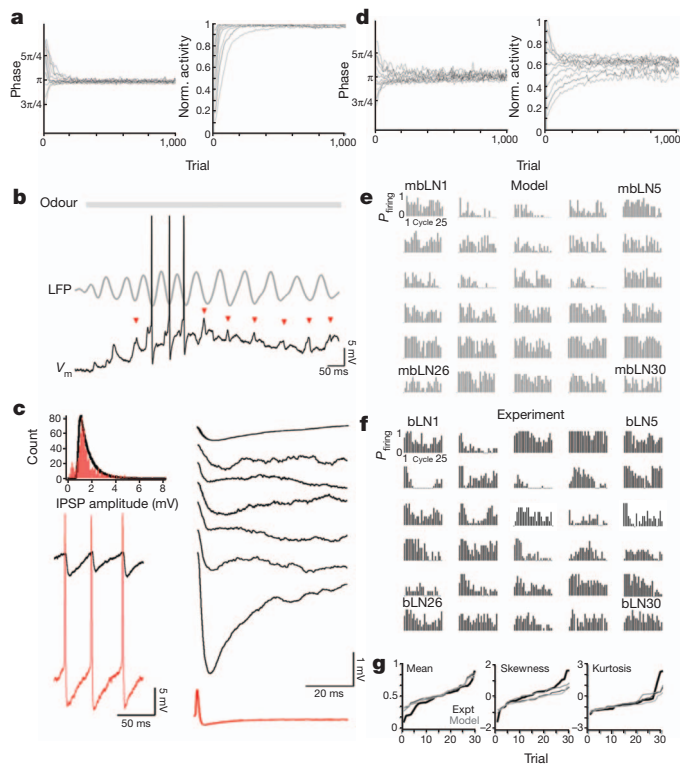


**Figure 2 | Saturation of activity caused by STDP can be counteracted by lateral inhibition.** **a**, Mean firing phase (left) and normalized population activity (right) in a simulation of a KC–bLN network (30 Izhikevich units<sup>44</sup>, one LFP cycle, 1,000 trials). Each point is a ten-trial average; STDP is turned on in trial 11. Each curve is run with  $n$  Kenyon cell inputs per mBLN ( $20 < n < 80$ , 10% connections in common). STDP regulates bLN firing phase (ref. 17) but inexorably drives bLN population to saturation. **b**, *In vivo* intradendritic recording of bLN membrane potential,  $V_m$ , together with LFP during odour presentation. Arrowheads indicate onsets of inhibitory postsynaptic potentials, timed on LFP troughs. **c**, Top left: frequency distribution of inhibitory postsynaptic potential amplitudes, measured at baseline, in 30 bLNs; black curve, fit used for model in **d**. IPSP, inhibitory postsynaptic potential. Bottom left: paired bLN recording revealing direct inhibitory connection. Right: bLN spike-triggered averages from seven distinct bLN pairs. **d**, Simulation of a bLN network as in **a**, except with  $n$  Kenyon cell inputs per bLN (here  $22 < n < 130$ , same drive at simulation onset as in **a**). Lateral inhibition among bLNs is as determined experimentally. Mean phase (left) is minimally affected; network activity (right) settles near midrange. **e**, Simulation of a bLN network as in **d**, extended over 25 LFP cycles, with time-varying Kenyon cell input profiles derived from experiments<sup>12,17,45</sup>. Post-stimulus time histograms plotted as firing probability versus cycle rank for each of the 30 mBLNs (ten trials), post STDP. **f**, *In vivo* intradendritic responses of 30 bLNs to *trans*-2-hexen-1-ol represented as in **e** (from 16 different animals). **g**, Comparison of experimental (black) and model (grey) bLN response statistics. Same simulation as in **e** (darkest grey) together with two other simulations of the same network with different Kenyon cell input profiles (lighter shades of grey).

### Conditional modulation of STDP rule

Mushroom bodies are critical for associative conditioning in insects<sup>6–11,27</sup>, and second-messenger pathways involved in memorization and retrieval have been described in *Drosophila*<sup>1,4–7,28,29</sup>. Yet we know little about the synaptic mechanisms underlying conditioning there<sup>30</sup>, and even less about how specificity is achieved or about the roles that STDP might have in it. Associative learning in insects seems to rely on neuromodulators<sup>31–35</sup> (for example octopamine (OCT) and dopamine) to mediate unconditioned signals (appetitive and aversive, respectively, for OCT and dopamine). In locusts and other insects, these neuromodulators are delivered nonspecifically by small numbers of octopaminergic<sup>36</sup> and dopaminergic<sup>37</sup> neurons with projections to the mushroom body lobes (among others), that is, where Kenyon cells contact bLNs.

We assessed the effect of local OCT injection into the  $\beta$ -lobes on plasticity and tuning of those bLNs *in vivo* (Fig. 3). Figure 3d illustrates our experimental schemes, which were designed to probe specificity, that is, the question of how the system determines which synapses should change when the reinforcer is global. During an odour stimulus, two features distinguish odour-evoked Kenyon cell spikes from ‘stray’ spikes produced randomly by non-responding Kenyon cells (most of the Kenyon cells): odour-evoked spikes are synchronized and cause bLNs to spike by their collective action. Hence, odour-evoked release at Kenyon cell synapses occurs within the time window for STDP. We thus tested the effect of OCT injection on synapses that differed only in their temporal features of pre- and postsynaptic activation. In each experiment, we measured the responses of one bLN to Kenyon cell stimulation at a rate of  $0.1 \text{ s}^{-1}$  at two locations (a pairing location (P) and a control location (C)) and two different times (C 300 ms before P). We found Kenyon cell stimulation sites that converged onto the same recorded bLN in 13 out of 20 experiments.

In ‘test’ trials (Fig. 3d, top), the bLN was depolarized by a brief pulse of current to produce one single action potential 5 s after Kenyon cell stimulation at P, hence well outside the window of  $\delta t = t_{\text{post}} - t_{\text{pre}} = \pm 25 \text{ ms}$  required for STDP<sup>17</sup>, where  $t_{\text{post}}$  and  $t_{\text{pre}}$  are respectively the post- and presynaptic spike times. Pairing consisted of five trials at  $0.1 \text{ s}^{-1}$ , of either of two kinds. In ‘STDP’ trials, the bLN was fired within  $\pm 25 \text{ ms}$  of a Kenyon cell stimulus at P (Fig. 3d, middle). In ‘STDP + OCT’ trials, pairing was as in STDP trials but was followed by one OCT injection (5 pl) 1 s after pairing (Fig. 3d, bottom). Test trials were carried out before STDP trials (Fig. 3a–c, red), after STDP trials (black) and after STDP + OCT trials (blue). All test and pairing trials thus contained the same numbers of pre- and postsynaptic pulses; only their relative timings differed. Examples with three values of  $\delta t$  are shown (Fig. 3a–c). In each, OCT caused a depression. We note that only connections between cells co-activated within the STDP window were depressed (that is, P but not C; see also Supplementary Fig. 6). The depressive action of OCT on synapses undergoing STDP (20 different values of  $\delta t$ ; Fig. 3e, f and Supplementary Fig. 7) was greatest for  $\delta t > 0$ , converting baseline Hebbian STDP into one where only depression occurred.

To rule out the possibility that the action of OCT resulted not from the pairing *per se*, but from the temporal proximity of OCT delivery to the pairing (P), we reversed the order of C and P ( $n = 3$ ; Supplementary Fig. 8). Again, only the P pathway was affected by OCT (effect of OCT on control (mean  $\pm$  s.e.m.):  $-0.9 \pm 0.49\%$ ,  $n = 3$  (P then C);  $0.2 \pm 2.28\%$ ,  $n = 10$  (C then P); sets statistically equivalent:  $P > 0.66$ , *t*-test). Hence, because the control and paired synapses shared the same postsynaptic partner (C and P differed only in the identity of the presynaptic cells and in the timings of the presynaptic spikes relative to those in their common bLN), and because the two sets of presynaptic cells were stimulated within only 300 ms of one another (C then P or P then C), we conclude that the relative timing of pre- and postsynaptic firing is what contributes to making the synapses susceptible to OCT action. We do not know whether pre–post delays longer than  $\pm 25 \text{ ms}$  (but shorter than 300 ms) would have equivalent effects. However, almost all odour-evoked Kenyon cell action potentials occur within the range of delays we tested. We conclude that, despite its global release, OCT affects specific synapses—those in which pre- and postsynaptic partners fired within the appropriate delay between one another. This is the case even though OCT was delivered 1 s after the relevant pairing (reproducing a temporal dissociation between conditioned stimulus and unconditioned stimulus<sup>14</sup>).

### Conditional changes of STDP are specific

The STDP curves in Fig. 3f were obtained *in vivo* with electrical activation of the pre- and postsynaptic cells. We next tested the effect of OCT on the responses of bLNs to odours. We predicted that if OCT depresses KC–bLN synapses that fire within the STDP time window,

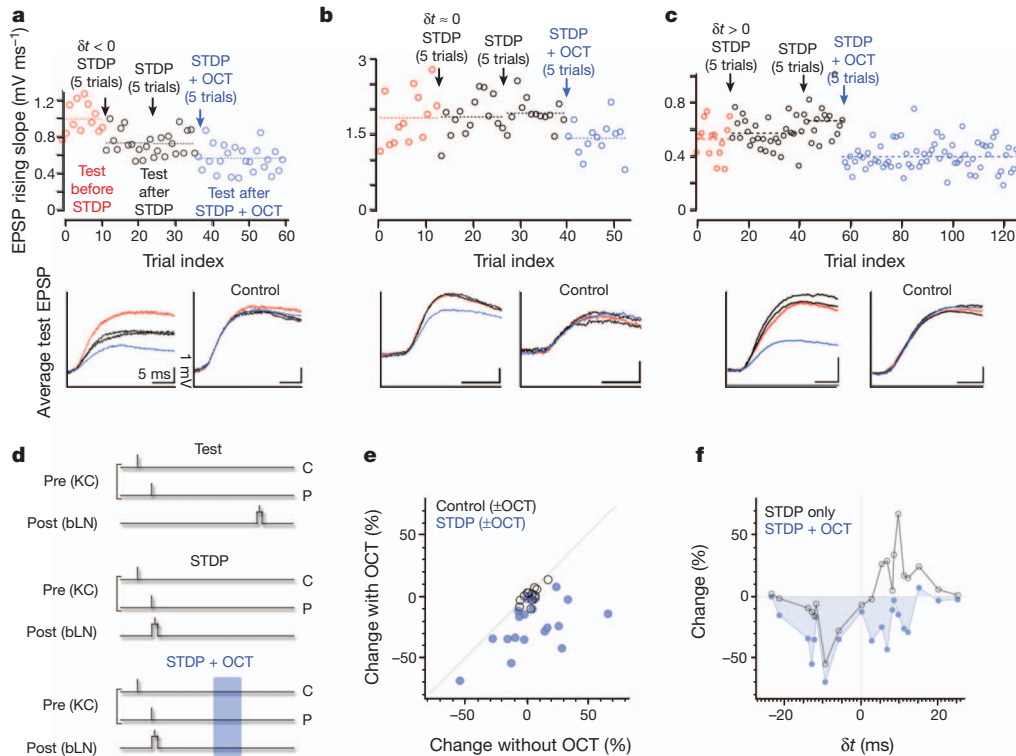


**Figure 3 | OCT changes the STDP rule.** **a**, Five trials pairing OCT with depressing STDP ( $\delta t < 0$ ) reduced KC–bLN excitatory postsynaptic potential (EPSP) size (blue) more than did two sets of five-trial STDP with negative  $\delta t$  alone (black). EPSPs evoked by interleaved stimulation with the control electrode (embedded among Kenyon cells in a different location) were unaffected (control, bottom right), despite equal exposure to OCT. **b**, Five trials pairing OCT with  $\delta t \approx 0$  STDP reduced KC–bLN EPSP size (blue), whereas STDP alone with this  $\delta t$  value had no effect (black). Control EPSPs were unaffected (bottom right). **c**, Five trials pairing OCT with potentiating STDP ( $\delta t > 0$ ) reduced KC–bLN EPSP size after it was potentiated by two bouts of STDP alone with this  $\delta t$  value. Control EPSPs were unaffected (bottom right). **d**, Stimulation protocols. Test trials were used to evaluate the amplitudes of KC–bLN EPSPs before STDP, after STDP and after STDP + OCT, as shown in **a–c**, and to compute (from multiple experiments) values in **e** and **f**. C, control Kenyon cell input; P, paired Kenyon cell input. In test trials, bLNs were depolarized with a 5-ms d.c. pulse (causing a single bLN spike)  $\sim 5$  s after

extracellular stimulation (0.1-ms pulses) of Kenyon cells in two different locations (C and P, 300 ms apart). In STDP trials, bLNs were depolarized as above, causing a single spike in a narrow window around the time of Kenyon cell stimulation (P). Control Kenyon cell stimulation (C) was offset by 300 ms. STDP + OCT trials were the same as STDP trials, only with the addition of localized OCT injection (50-ms pressure-pulse) in the  $\beta$ -lobe, 1 s after P Kenyon cell stimulation. **e**, Summary data from 20 experiments, plotting for each experiment the effect of STDP + OCT versus STDP alone (blue dots) and plotting control data, with and without OCT, for 13 of 20 experiments (black circles). Changes due to STDP + OCT differ significantly from control + OCT ( $P < 0.003$ ,  $t$ -test). Changes due to OCT in control not significantly different from zero ( $P > 0.84$ ,  $t$ -test; see also Supplementary Fig. 7). **f**, Comparison between change due to STDP + OCT and change due to STDP alone, each plotted as a function of  $\delta t$ . Changes due to STDP + OCT differ significantly from zero (relative to before STDP:  $P < 0.0001$ ; relative to STDP only:  $P < 0.0002$ ,  $t$ -test; see also Supplementary Fig. 7).

it should also reduce bLN output. This was tested first with our model, using an STDP rule modified according to Fig. 3f: responses were reduced in 28 of 30 mBLNs (Fig. 4a, b). We then tested the prediction experimentally with 12 bLNs (18 bLN–odour pairs), each recorded intracellularly from a dendrite. In 16 of 18 instances, OCT caused a reduction of bLN output, averaged over the odour response (Fig. 4c, d). LFP power in the mushroom body calyx was unaffected (Fig. 4f), consistent with unchanged input to the mushroom body.

We also evaluated the specificity of changes in bLN–odour responses. A bLN was presented with three odours in blocks of trials in the order indicated (Fig. 4e, left). OCT was injected 800 ms after odour onset, paired each time with only one of the three odours. As in Fig. 4c, d, the responses of the bLN to the three odours (assembled by odour in three graphs; Fig. 4e, right) were reduced after pairing with OCT (compare blue and red post-stimulus time histograms). The reduction of the response to an odour occurred only after pairing of that particular odour with OCT. For example, responses to cherry and *trans*-2-hexen-1-ol were minimally affected by pairing OCT with 2-heptanone; they became significantly reduced only after the appropriate pairing of either cherry or *trans*-2-hexen-1-ol with OCT. Figure 4f compares summary data for odours paired with OCT ( $n = 18$  bLN–odour pairs) to controls ( $n = 12$  bLN–odour pairs:

odour responses after pairing of a different odour with OCT ( $n = 7$ ) and odour responses after pairing of electrical Kenyon cell stimulation with OCT ( $n = 5$ );  $n = 18$  LFP recordings simultaneous with intracellular bLN recordings). These results support the observation that OCT specifically depresses contacts between cells co-activated within the STDP window (Fig. 3); they also indicate that KC–bLN pairing and OCT should co-occur within an interval of at most a few tens of seconds.

## Discussion

In the absence of OCT, STDP at KC–bLN synapses adaptively regulates the bLN spike phase<sup>17</sup> and bLN population output, helped by the action of lateral inhibition between bLNs (Fig. 2). In the context of reinforcer delivery, STDP gains a new role: it tags—presumably through biochemical changes dependent on pairing—the synapses between connected Kenyon cells and bLNs that have fired an action potential within the STDP pairing window, itself commensurate with the oscillation period in this system<sup>38</sup>. This renders those synapses susceptible to the action of OCT (which is proposed to mediate positive reinforcement in insect learning<sup>14,34,39</sup>) and reduces the inhibitory output of the mushroom body mediated by bLNs. Hence, the action of OCT can be specific, even though its release is diffuse and often delayed

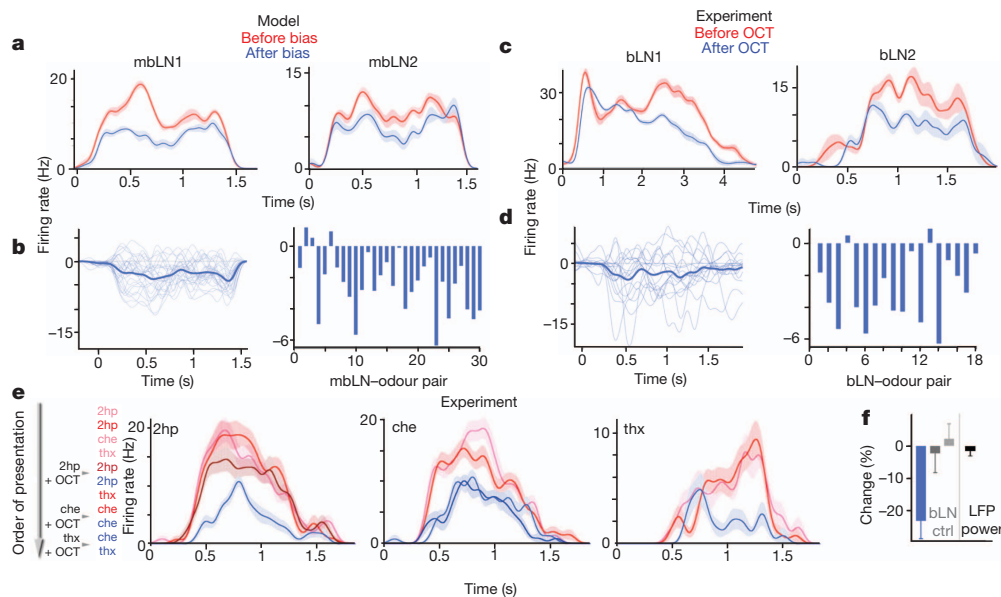


**Figure 4 | Odour-specific decrease of mushroom body output by OCT.**

**a**, Simulation of bLN network as in Fig. 2e. Smoothed post-stimulus time histograms (PSTHs) for two mbLNs (ten trials; shading, s.e.). Red, responses at equilibrium; blue, responses after ten trials with STDP + OCT curve shown in Fig. 3f. **b**, Left: difference in PSTHs for all 30 mbLN responses before and after five trials of STDP + OCT ('PSTH after pairing' minus 'PSTH before pairing', thin lines). Responses of individual units at particular times can increase or decrease, but average difference (thick line) is less than zero at all times. Right: time-averaged differences for each of the 30 mbLNs ('PSTH after pairing' minus 'PSTH before pairing'). In some instances, mbLN responses increased (for most units this occurred transiently; for a few mbLNs the entire time-averaged response increased). This is due to reduced lateral inhibition (that is, disinhibition) because mbLN population activity decreased. **c**. *In vivo* intradendritic recordings of bLN odour responses before and after pairing of the odour with localized OCT injection in the  $\beta$ -lobe (50-ms pressure-pulse, 800 ms after odour onset, either five ( $n = 5$ ) or ten pairing trials ( $n = 13$ )). PSTHs for two bLNs (ten trials; shading, s.e.): red, responses before odour-OCT pairing; blue, responses after ten trials of odour paired with OCT injection. **d**, Same difference of PSTHs as in **b**, for 18 recorded bLN-odour pairs (12 bLNs). As in the model, responses of individual bLNs can increase or

decrease transiently, but on average there is a net decrease. **e**, OCT-induced changes are odour specific. Three odours are sequentially paired (during five trials) with OCT to assess carry-over of pairing across odours. Order of stimuli is shown at left. Red colours, responses before pairing with OCT; blue colours, responses after pairing. Odours are presented in ten-trial blocks and PSTHs are shown for each block (shading, s.e.). Changes due to nonspecific pairing are minimal by comparison with those due to odour-specific pairing. **f**, Summary data comparing the effect of odour-OCT pairing (blue:  $n = 18$  bLN-odour pairs, 12 bLNs) with those of controls (grey:  $n = 12$  bLN-odour pairs, 9 bLNs; black (LFP controls):  $n = 18$  recordings simultaneous with intracellular bLN recordings). Dark grey ( $n = 7$ ), effect on bLN response to non-paired odour before and after pairing another odour with OCT. Light grey ( $n = 5$ ), effect on bLN response to non-paired odour before and after pairing electrical activation of Kenyon cells with OCT. Black, effect on LFP power (10–30-Hz band, recorded in mushroom body) before and after pairing odour with OCT. Changes due to pairing odour with OCT differ significantly from zero ( $P < 0.0006$ ,  $t$ -test) and from those in the three control conditions ( $P < 0.002$ – $0.022$ ,  $t$ -test). Changes in control conditions were not significantly different from zero ( $P > 0.72$  (dark grey),  $0.64$  (light grey) and  $0.33$  (black)).

relative to the conditioned (odour) stimulus. This provides experimental support for related theoretical propositions<sup>23,40,41</sup>. Our results also solve the temporal dissociation puzzle revealed in experiments<sup>14</sup>.

Because the selectivity of synaptic change allowed by STDP relies on the rare co-occurrence of pre- and postsynaptic spikes, it is beneficial that Kenyon cell firing is rare and that odour representations by Kenyon cells are sparse, as observed<sup>12–14</sup>. We propose that olfactory associative memories are stored, at least in part, as sparse sets of synaptic weights between Kenyon cells and mushroom body output neurons. In the absence of reinforcer, STDP and lateral inhibition between bLNs set the (default) instantaneous output of the  $\beta$ -lobe network near the middle of its dynamic range. This serves at least two purposes. First, it maximizes the number of possible distinct combinations of simultaneously active bLNs. Second, it ensures that the output of the network can be increased or decreased, if an associative reinforcer is to co-occur. It is possible that some of the molecular pathways revealed by *Drosophila* neurogenetics<sup>6,9,11</sup> have a role in the phenomenon described here. The functional form of STDP has recently been shown to depend on neuromodulatory context in mammalian brain slices<sup>22,42,43</sup>, suggesting that our results may have broad implications for STDP and learning.

## METHODS SUMMARY

All results were obtained *in vivo* from locusts housed in a crowded colony. Odours were delivered by injection of a controlled volume of odorized air within a

constant stream of desiccated air. The results presented here are derived from intradendritic recordings, made using sharp micropipettes, of 76 neurons in 55 locusts. LFPs were recorded with silicon probes (NeuroNexus) in the mushroom body Kenyon cell soma cluster. Octopamine (100  $\mu$ M) was injected locally into the mushroom body  $\beta$ -lobe using a picopump (WPI). Electrical stimulation of Kenyon cell somata was done with modified tetrodes (FHC). Stimulation protocols and data analysis were carried out using specialized software (LABVIEW, National Instruments; IGOR, Wavemetrics; and MC\_STIMULUS, Multichannel Systems). Simulations of networks of 'Izhikevich units'<sup>44</sup> were done using MATLAB (Mathworks).

**Full Methods** and any associated references are available in the online version of the paper at [www.nature.com/nature](http://www.nature.com/nature).

Received 16 September; accepted 8 December 2011.

Published online 25 January 2012.

- McGuire, S. E., Le, P. T. & Davis, R. L. The role of *Drosophila* mushroom body signaling in olfactory memory. *Science* **293**, 1330–1333 (2001).
- Tully, J. B. C. T. in *Drosophila: A Practical Approach* (ed. Roberts, D. B.) 265–317 (Oxford Univ. Press, 1998).
- de Belle, J. S. & Heisenberg, M. Associative odor learning in *Drosophila* abolished by chemical ablation of mushroom bodies. *Science* **263**, 692–695 (1994).
- Tully, T. & Quinn, W. G. Classical conditioning and retention in normal and mutant *Drosophila melanogaster*. *J. Comp. Physiol. A* **157**, 263–277 (1985).
- Heisenberg, M., Borst, A., Wagner, S. & Byers, D. *Drosophila* mushroom body mutants are deficient in olfactory learning. *J. Neurogenet.* **2**, 1–30 (1985).
- Quinn, W. G., Harris, W. A. & Benzer, S. Conditioned behavior in *Drosophila melanogaster*. *Proc. Natl Acad. Sci. USA* **71**, 708–712 (1974).

7. Keene, A. C. & Waddell, S. *Drosophila* olfactory memory: single genes to complex neural circuits. *Nature Rev. Neurosci.* **8**, 341–354 (2007).
8. Akalal, D. B. *et al.* Roles for *Drosophila* mushroom body neurons in olfactory learning and memory. *Learn. Mem.* **13**, 659–668 (2006).
9. Davis, R. L. Olfactory memory formation in *Drosophila*: from molecular to systems neuroscience. *Annu. Rev. Neurosci.* **28**, 275–302 (2005).
10. Gerber, B., Tanimoto, H. & Heisenberg, M. An engram found? Evaluating the evidence from fruit flies. *Curr. Opin. Neurobiol.* **14**, 737–744 (2004).
11. Heisenberg, M. Mushroom body memoir: from maps to models. *Nature Rev. Neurosci.* **4**, 266–275 (2003).
12. Perez-Orive, J. *et al.* Oscillations and sparsening of odor representations in the mushroom body. *Science* **297**, 359–365 (2002).
13. Turner, G. C., Bazhenov, M. & Laurent, G. Olfactory representations by *Drosophila* mushroom body neurons. *J. Neurophysiol.* **99**, 734–746 (2008).
14. Ito, I., Ong, R. C.-Y., Raman, B. & Stopfer, M. Sparse odor representation and olfactory learning. *Nature Neurosci.* **11**, 1177–1184 (2008).
15. Kanerva, P. *Sparse Distributed Memory* (MIT Press, 1988).
16. Papadopoulou, M., Cassenaer, S., Nowotny, T. & Laurent, G. Normalization for sparse encoding of odors by a wide-field interneuron. *Science* **332**, 721–725 (2011).
17. Cassenaer, S. & Laurent, G. Hebbian STDP in mushroom bodies facilitates the synchronous flow of olfactory information in locusts. *Nature* **448**, 709–713 (2007).
18. Markram, H., Lübke, J., Frotscher, M. & Sakmann, B. Regulation of synaptic efficacy by coincidence of postsynaptic APs and EPSPs. *Science* **275**, 213–215 (1997).
19. Bi, G. Q. & Poo, M. M. Synaptic modifications in cultured hippocampal neurons: dependence on spike timing, synaptic strength, and postsynaptic cell type. *J. Neurosci.* **18**, 10464–10472 (1998).
20. Abbott, L. F. & Nelson, S. B. Synaptic plasticity: taming the beast. *Nature Neurosci.* **3**, 1178–1183 (2000).
21. Meeks, J. P. & Holy, T. E. Pavlov's moth: olfactory learning and spike-timing-dependent plasticity. *Nature Neurosci.* **11**, 1126–1127 (2008).
22. Pawlak, V. *et al.* Timing is not everything: neuromodulation opens the STDP gate. *Front. Syn. Neurosci.* **2**, 146 (2010).
23. Izhikevich, E. M. Solving the distal reward problem through linkage of STDP and dopamine signaling. *Cereb. Cortex* **17**, 2443–2452 (2007).
24. Gütiğ, R., Aharonov, R., Rotter, S. & Sompolinsky, H. Learning input correlations through nonlinear temporally asymmetric Hebbian plasticity. *J. Neurosci.* **23**, 3697–3714 (2003).
25. Huerta, R., Nowotny, T., Garcia-Sanchez, M., Abarbanel, H. D. I. & Rabinovich, M. I. Learning classification in the olfactory system of insects. *Neural Comput.* **16**, 1601–1640 (2004).
26. Masquelier, T. & Thorpe, S. J. Unsupervised learning of visual features through spike timing dependent plasticity. *PLoS Comput. Biol.* **3**, e31 (2007).
27. Waddell, S. & Quinn, W. G. Learning how a fruit fly forgets. *Science* **293**, 1271–1272 (2001).
28. Isabel, G., Pascual, A. & Preat, T. Exclusive consolidated memory phases in *Drosophila*. *Science* **304**, 1024–1027 (2004).
29. Gervasi, N., Tchénio, P. & Preat, T. PKA dynamics in a *Drosophila* learning center: coincidence detection by rutabaga adenyl cyclase and spatial regulation by dunce phosphodiesterase. *Neuron* **65**, 516–529 (2010).
30. Wang, Y., Mamiya, A., Chiang, A. S. & Zhong, Y. Imaging of an early memory trace in the *Drosophila* mushroom body. *J. Neurosci.* **28**, 4368–4376 (2008).
31. Claridge-Chang, A. *et al.* Writing memories with light-addressable reinforcement circuitry. *Cell* **139**, 405–415 (2009).
32. Kim, Y. C., Lee, H. G. & Han, K. A. D1 dopamine receptor dDA1 is required in the mushroom body neurons for aversive and appetitive learning in *Drosophila*. *J. Neurosci.* **27**, 7640–7647 (2007).
33. Riemensperger, T., Voller, T., Stock, P., Buchner, E. & Fiala, A. Punishment prediction by dopaminergic neurons in *Drosophila*. *Curr. Biol.* **15**, 1953–1960 (2005).
34. Schwaerzel, M. *et al.* Dopamine and octopamine differentiate between aversive and appetitive olfactory memories in *Drosophila*. *J. Neurosci.* **23**, 10495–10502 (2003).
35. Mizunami, M. & Matsumoto, Y. Roles of aminergic neurons in formation and recall of associative memory in crickets. *Front. Behav. Neurosci.* **4**, 172 (2010).
36. Braunig, P. Suboesophageal DUM neurons innervate the principal neuropiles of the locust brain. *Phil. Trans. R. Soc. Lond. B* **332**, 221–240 (1991).
37. Wendt, B. & Homberg, U. Immunocytochemistry of dopamine in the brain of the locust *Schistocerca gregaria*. *J. Comp. Neurol.* **321**, 387–403 (1992).
38. Laurent, G. & Naraghi, M. Odorant-induced oscillations in the mushroom bodies of the locust. *J. Neurosci.* **14**, 2993–3004 (1994).
39. Hammer, M. An identified neuron mediates the unconditioned stimulus in associative olfactory learning in honeybees. *Nature* **366**, 59–63 (1993).
40. Gütiğ, R. & Sompolinsky, H. The tempotron: a neuron that learns spike timing-based decisions. *Nature Neurosci.* **9**, 420–428 (2006).
41. Huerta, R. & Nowotny, T. Fast and robust learning by reinforcement signals: explorations in the insect brain. *Neural Comput.* **21**, 2123–2151 (2009).
42. Seol, G. H. *et al.* Neuromodulators control the polarity of spike-timing-dependent synaptic plasticity. *Neuron* **55**, 919–929 (2007).
43. Shen, W., Flajolet, M., Greengard, P. & Surmeier, D. J. Dichotomous dopaminergic control of striatal synaptic plasticity. *Science* **321**, 848–851 (2008).
44. Izhikevich, E. M. Simple model of spiking neurons. *IEEE Trans. Neural Netw.* **14**, 1569–1572 (2003).
45. Mazor, O. & Laurent, G. Transient dynamics versus fixed points in odor representations by locust antennal lobe projection neurons. *Neuron* **48**, 661–673 (2005).

**Supplementary Information** is linked to the online version of the paper at [www.nature.com/nature](http://www.nature.com/nature).

**Acknowledgements** This work was funded by the Lawrence Hanson Chair at Caltech, the National Institutes on Deafness and other Communication Disorders, Caltech's Broad Fellows Program, the Office of Naval Research (grants N00014-07-1-0741 and N00014-10-1-0735) and the Max Planck Society. We are grateful to L.-P. Mok for help with locust dissections and to E. Schuman, A. Siapas, E. Lubenov, M. Papadopoulou and members of the Laurent lab for comments on the manuscript.

**Author Contributions** S.C. and G.L. designed the experiments and simulations, discussed the results and wrote the paper. S.C. carried out the experiments and simulations.

**Author Information** Reprints and permissions information is available at [www.nature.com/reprints](http://www.nature.com/reprints). The authors declare no competing financial interests. Readers are welcome to comment on the online version of this article at [www.nature.com/nature](http://www.nature.com/nature). Correspondence and requests for materials should be addressed to G.L. ([gilles.laurent@brain.mpg.de](mailto:gilles.laurent@brain.mpg.de)) or S.C. ([stijn@caltech.edu](mailto:stijn@caltech.edu)).

## METHODS

**Preparation and stimuli.** All results were obtained *in vivo* from locusts (*Schistocerca americana*) housed in an established, crowded colony. Young adults of either sex were immobilized in a holder. Both antennae were secured in place with respect to the olfactory delivery system and remained intact for olfactory stimulation. The brain was exposed, desheathed and superfused with locust saline, as previously described<sup>38</sup>.

**Odour delivery.** Odours were diluted 10% v/v in paraffin oil. They were delivered by injection of a controlled volume of odorized air within a constant stream of desiccated air. Total airflow was set to 0.85 l min<sup>-1</sup> and the odour was further diluted by one-third in air. Teflon tubing was used at and downstream of the mixing point to prevent odour lingering and cross-contamination.

**Intradendritic recordings.** Sharp electrode recordings from the dendrites of bLNs were made with borosilicate glass micropipettes (d.c. resistance, 150–200 MΩ) filled with 1 M potassium acetate. The cell type from which the data are derived could be recognized by several characteristics: responses to odour, subthreshold baseline activity profile and response to electrical stimulation of Kenyon cells<sup>17</sup>. Recordings from bLNs were always made from dendrites in the β-lobe. To assess changes in bLN instantaneous firing rate, bLN spike times were either binned per simultaneously recorded LFP cycle (Fig. 2f) or convolved with a 50-ms Gaussian kernel to generate smoothed PSTHs (Fig. 4c, e; shading, s.e.). EPSP slope was measured as the maximum slope over the 10–90% range of maximum amplitude. The average EPSP waveforms shown at bottom in Fig. 3a–c were computed from the same data as the slope measurements shown at top in Fig. 3a–c. The electrical stimulation rate was 0.1 s<sup>-1</sup> (with no intertrial gap). The results in this work were obtained from 55 animals; in two instances the same animal was used for two distinct bLNs with OCT injection.

**LFP recordings.** LFPs were recorded in the mushroom body Kenyon cell soma layer using Michigan probes (<http://www.neuronexustech.com>).

**Electrical stimulation.** Twisted-wire tetrodes obtained from FHC (no. CE4B75) were modified for monopolar stimulation, with the casing serving as the anode. The tips of the tetrodes were splayed such that the distance between the exposed tips was approximately equal to 60% of the diameter of the mushroom body calyx. The exposed end of the stimulating electrode was embedded among Kenyon cell somata. The tetrodes were electroplated with gold solution to impedances of 200–350 kΩ at 1 kHz. Stimulating currents (5–140 μA, 0.1 ms) were generated using an STG1000 Multichannel System (as in ref. 17).

**OCT injection.** Patch pipettes were back-filled with a 100 μM OCT hydrochloride, 0.01% Fast Green solution. A pneumatic picopump (WPI) was used to apply one 50-ms, 5-p.s.i. pressure pulse per trial. Each pulse injected ~5 pl (as measured by previous injection into a drop of oil). The injected solution was localized to the β-lobe, as verified by bounded diffusion of the Fast Green dye.

**Simulations.** All simulations were carried out with networks of Izhikevich units<sup>44</sup>. Networks consisted of 30 units each with dynamics given by

$$\frac{dv}{dt} = 0.04v^2 + 5v + 140 - u + I$$

$$\frac{du}{dt} = a(bv - u)$$

where  $a = 0.02$ ,  $b = 0.2$ ,  $c = -65$ ,  $d = 8$  and if  $v \geq 30$  then  $v \leftarrow c$  and  $u \leftarrow u + d$ . Synaptic interactions and external inputs were introduced through the  $I$  term, which for the  $j$ th unit takes the form

$$I_j = \sum_i w_{\text{bLN}}(i,j)f_{\text{bLN}}(i) + \sum_k w_{\text{KC}}(k,j)f_{\text{KC}}(k)$$

Here  $w_{\text{bLN}}$  is a matrix of inhibitory weights among network units,  $f_{\text{bLN}}$  is the vector of spike times generated by the network,  $w_{\text{KC}}$  is a matrix of excitatory input weights and  $f_{\text{KC}}$  is the vector of spike times that constitutes the input to the network. At every trial,  $f_{\text{KC}}$  is drawn from a distribution characterized by three experimental observations: odour-evoked Kenyon cell spiking phase distribution relative to the LFP<sup>12</sup>, average odour-evoked Kenyon cell population PSTH<sup>45</sup> and Kenyon cell baseline activity<sup>12</sup>. The matrix  $w_{\text{bLN}}$  is estimated from experimental recordings and kept fixed during the simulation. The matrix  $w_{\text{KC}}$  is drawn from a normal distribution at the onset of the simulation, with variable means for different initial conditions; it is updated in every trial according to

$$\Delta w = \begin{cases} \lambda f_{-}(w)K(\Delta t) & \text{if } \Delta t \leq 0 \\ \lambda f_{+}(w)K(\Delta t) & \text{if } \Delta t > 0 \end{cases}$$

The temporal filter,  $K(\Delta t)$ , is the experimentally derived STDP curve: either the unbiased Hebbian form as in ref. 17 or the depression-biased form that results from pairing with OCT as in Fig. 3f. The learning rate was set by the number of pairings carried out to arrive at the STDP curve in experiments. The weight dependences of the updating functions  $f_{+}(w)$  and  $f_{-}(w)$  are as follows:

$$f_{+}(w) = (1 - w)^{\mu}$$

$$f_{-}(w) = w^{\mu}$$

As described in ref. 24, the value of  $\mu$  determines the shape of the equilibrium weight distribution. A value ( $\mu = 0.08$ ) was chosen such that the weight distribution in the simulation at equilibrium matched the experimental EPSP size distribution (Supplementary Information, section 3). As described above, parameters in the model were constrained by experimental estimates, except for  $a$ ,  $b$ ,  $c$  and  $d$ , which characterize the dynamics of individual model units. These parameters took the typical values used for regular spiking neurons<sup>44</sup>.

## CORRIGENDUM

doi:10.1038/nature11261

### Corrigendum: Conditional modulation of spike-timing-dependent plasticity for olfactory learning

Stijn Cassenaer & Gilles Laurent

*Nature* **482**, 47–52 (2012); doi:10.1038/nature10776

In this Article, two of the 30 plots in Fig. 2f were inadvertently duplicated from the corresponding panels in Fig. 2e. The corrected figure is shown below (with the two corrected panels boxed). The error has been corrected online in the HTML and PDF of the original paper.

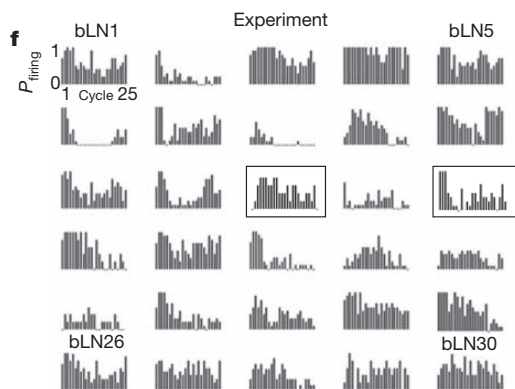


Figure 1 | This is the corrected Fig. 2f of the original Article.